RSC Advances

PAPER

View Article Online
View Journal | View Issue

Cite this: *RSC Adv.*, 2017, **7**, 25437

Metal ion type significantly affects the morphology but not the activity of lipase–metal–phosphate nanoflowers†

N. Sharma, ‡[a] M. Parhizkar,[a] W. Cong,[a] Srikanth Mateti,[a] M. A. Kirkland,[a] M. Puri[b] and A. Sutti ‡*[a]

Received 9th January 2017
Accepted 14th April 2017

DOI: 10.1039/c7ra00302a

rsc.li/rsc-advances

Enzyme–metal-ion–phosphate nanoflowers are high-surface area materials which are known to show higher activity than the constituting protein. Although the synthesis of hybrid nanoflowers has been demonstrated with a variety of proteins and reaction conditions, only di-valent metal ions have been tested to date. We expand on previous findings by testing a range of metal ions of different valence in co-presence with lipase from *Burkholderia cepacia*: Ag(I), Fe(II), Cu(II), Au(III). All metal ions produced colour precipitates, although the type of metal caused different precipitate morphologies under comparable reaction conditions: from nanoflowers to forests of nano-plates and crystal-like precipitates. In contrast, the type of metal ion did not appear to significantly affect the product's specific enzyme activity, which remained greater than that of free lipase. This indicates that the type of metal ion and the macroscopic arrangement of the petals play a secondary role to that of the co-presence of the metal and phosphate ions in determining lipase nanoflower activity. The demonstrated ability to produce metal–phosphate-protein nanoflowers with a selection of different metals also opens the way to producing a wider range of functional, nanostructured, materials.

Introduction

Lipases are glycerol ester hydrolases that have been used to catalyse esterification and transesterification in organic solvents. Accordingly, they have found widespread use in pharmaceuticals, textiles, food, dairy, detergents, paper industry, cosmetics and various fragrances.[1–5] However, the instability of free enzymes in aqueous solutions limits their use in industrial applications. Two standard methods, chemical modification and immobilisation, have been used extensively[6,7] to enhance the enzymes' catalytic activity, reusability, and long-term stability. Although chemically modified enzymes have exhibited improved stability, they have not demonstrated a significant improvement in catalytic activity.[6,8,9]

In contrast to chemical modification, the immobilisation of enzymes onto a suitable support is a simpler and more widely applicable solution.[10] Immobilised enzymes present several advantages over free enzymes, such as improved reusability, long-term stability and lower enzyme consumption in processes.[1,7,11–15] Various materials have been utilised as supports for enzyme immobilisation including mesostructures, sol–gel materials and organic or inorganic nanomaterials to which the enzymes are bound *via* adsorption, covalent attachment, entrapment or cross-linking.[16–24] Nanomaterials have shown potential as supports for immobilised enzymes and have been shown to improve the efficacy of biocatalysts.[19–24] Large surface-to-volume ratio, higher enzyme loading and improved catalytic activity are typical characteristics of immobilised enzymes.[18] Immobilised lipases can be reused, therefore lowering the cost of enzyme-based processing.

Protein–inorganic hybrid nanostructures with flower-like shapes (nanoflowers) have been prepared using a variety of proteins and a bio-inspired approach, taking advantage of a complexation reaction between metal phosphates and proteins.[25–29] When enzymes were used as the protein component, the nanoflowers exhibited increased enzymatic activity and stability compared to the free enzyme. This was attributed to the high surface area and confinement of enzymes in the nanoflowers.[25–29] Wu, *et al.* investigated the synthesis of lipase-based nanoflowers and successfully utilised these for efficient transesterification of chiral alcohols (*R*,*S*)-2-pentanol.[30] Ozdemir, *et al.* utilised the same reaction scheme to synthesise horseradish peroxidase-based hybrid nanoflowers for detection of phenol.[27] Yang, *et al.* also reported synthesising enzyme–inorganic nanoflowers and using them as sensors for visual detection of hydrogen peroxide and phenol.[26]

[a]*Deakin University, Institute for Frontier Materials, 75 Pigdons Rd, Waurn Ponds, Geelong, VIC 3228, Australia. E-mail: asutti@deakin.edu.au*

[b]*Deakin University, School of Life and Environmental Sciences, 75 Pigdons Rd, Waurn Ponds, VIC 3228, Australia. E-mail: Munish.puri@deakin.edu.au*

† Electronic supplementary information (ESI) available. See DOI: 10.1039/c7ra00302a

‡ These authors are to be considered as equal first authors.

The technique is still relatively new and factors that influence the formation of enzyme–metal phosphate nanoflowers remain to be well described. For instance, most studies on the formation of protein-metal phosphate nanoflowers have focused on the use of cupric and calcium ions, but there is little evidence of the use of other metal ions,[31] in particular with valence other than 2+. It is important to assess whether metal ions other than copper and calcium may be used to form hybrid nanoflowers, because some enzymatic reactions might benefit from the co-presence of specific ions, resulting in nanoflowers with greatly enhanced enzymatic activity.[31] Additionally, it is to be verified whether the use of different metal ions, within the same group on the periodic table but with different valence, might result in different structural features, working in different reaction conditions, or even enzymatic activity advantages.

Further investigation is therefore needed to explore the effects of incubation parameters and metal ions on the morphology of nanoflowers as well as the influence of structure on catalytic activity and enzyme stability. Given the ample choice in applications for lipases, and promising reports on lipase nanoflower activity,[32] lipase was chosen as a model for this study. This study focused on the formation, catalytic activity, and stability of hybrid nanoflowers containing lipase from *Burkholderia cepacia* (BCL), prepared using four different metal ions – iron(II), copper(II), silver(I) and gold(III). The last three metal ions belong to the same group in the d-block of the periodic table, while iron(II) carries the same charge as copper(II) and is here used as same-charge comparison. The primary objective of the study was to identify the effect of process parameters on the formation of nanoflowers and to investigate enzyme activity and stability against different substrates for a range of different nanoflowers.

Experimental

Materials

Lipase (EC 3.1.1.3) from *Burkholderia cepacia* (BCL), bovine serum albumin solution (Aldrich: Protein Standard, analytical, 200 mg mL^{-1}), copper(II) sulfate pentahydrate, ferrous(II) sulfate, silver(I) nitrate, gold(III) chloride, polynitrophenol palmitate and salts (NaCl, KCl, Na_2HPO_4, KH_2PO_4, $CaCl_2 \cdot 2H_20$, and $MgCl_2 \cdot 6H_2O$) were obtained from Sigma-Aldrich (St. Louis, US). Deionised water was used in all experiments.

Synthesis of lipase-containing nanoflowers

The lipase nanoflowers (hNFs) were synthesised according to published methods, with slight modifications.[25] 15–75 μl of aqueous 120 mM $CuSO_4$, $FeSO_4$, $AgNO_3$, $HAuCl_4$ solutions were added to 9 mL of PBS (pH 7.4), containing 0.02 mg mL^{-1} lipase, to obtain a final metal ion concentration of 0.2–1 mM. The mixture was vigorously shaken using a Vortex mixer (Ratek), followed by incubation without agitation for 72 h at 4°C or room temperature (21 ± 3°C). The influence of metal-ions was studied by varying the metal ion concentration in the range from 0.2 to 1 mM. After incubation, yellow, blue, brown and purple precipitates were observed at the bottom of the reaction tubes, respectively for: ferrous-lipase, copper-lipase, silver-lipase, and gold-lipase samples. The precipitates were collected after centrifugation at 7000 rpm for 15 min, on Eppendorf 5430R centrifuge, equipped with rotor 5430R. The supernatant was removed, the precipitates were re-dispersed in deionised water and centrifuged at the same speed three times to remove unreacted components. Finally, the precipitates were dried at room temperature.

Lipase activity and content assays

The enzyme assay was performed according to published methods,[33] with some modification. The reaction mixture contained 2.7 mL of 50 mM phosphate buffer (pH 6.5), 0.3 mL of 50 mM p-nitrophenyl palmitate (pnp as substrate) in 2-propanol, 1 mg of hNFs powder (with equal amounts corresponding to free enzyme for the positive control), and 100 mM sodium carbonate (Na_2CO_3). The reaction mixture was incubated at 37°C for 10 min. The released p-nitrophenol was measured by UV-Vis spectrophotometer at 420 nm and its concentration calculated from a standard curve collected for p-nitrophenol. One unit of enzyme activity is here defined as 1 μmol of p-nitrophenol liberated per minute under standard assay (pH 6.5, 37 °C). All experiments were carried out in triplicate and the mean values were expressed ±SD. The specific activity (U) was defined as the amount of p-nitrophenol produced per mg of the nanoflowers. Stability measurements were performed for both free enzyme and immobilised lipase hNFs after storing the samples at 4 °C and room temperature (21 °C).

The Bradford reagent test was performed to assess the amount of protein present in the supernatant for each sample, before and after reaction. Bovine serum albumin was used as a standard protein.[34] 0.1 mL of each sample was added to the test tube and mixed with 1 mL of Bradford reagent as in the standard method. The immobilisation yield of protein was determined as described in the literature.[35]

Characterisation of the nanoflowers

Scanning electron microscopy (SEM) images were obtained using a Supra Zeiss 55vp. For the analyses, the powders were deposited on SEM sample stubs in two ways: dry powders were deposited on adhesive carbon tape, wet aqueous suspensions were dried on an aluminium stub. The samples were sputter-coated with gold/carbon on a Leica ACE 600. Finally, SEM and Energy-dispersive X-ray spectroscopy (EDX) analyses were performed to study the morphology and composition using a Zeiss Supra 55VP microscope, equipped with a Zeiss Supra 55vp EDX detector (Oxford instruments X-Max). TEM: bright field images were acquired on a JEOL 2100 LaB_6 transmission electron microscope, working at or below 200 KV. The structure of the samples was studied with X-ray powder diffraction (XRD) using a PANalytical X'Pert Pro powder diffractometer (Cu K-alpha radiation, $\lambda = 0.15418$ nm) with an applied voltage of 40 kV and a current of 30 mA, spectra were acquired over the 2θ range 7° to 50° with 0.02° step size and 150 s per step acquisition time.

Fourier Transform Infrared Spectroscopy (FTIR) was conducted in attenuated total reflection (ATR) mode using a Bruker Optics Vertex 70 instrument.

Reusability and stability test

The reusability of the immobilised lipase hNFs was assessed by carrying out the hydrolysis of a long chain ester (p-NP palmitate, pnp) under standard assay conditions as described above. After each cycle, the hNFs were separated from the reaction solution by centrifugation and rinsed with assay buffer. In running the next cycle, the hNFs were re-suspended in fresh buffer and added to fresh p-NP palmitate (0.3 mL). The activity of the immobilised hNFs after the first cycle was considered as the control and attributed a relative activity of 100%.

The same standard assay was performed after storing the hNFs at different storage temperatures 4 °C and 21 °C. First, enzyme-equivalent concentrations of hNFs and free lipase were dissolved in 2.7 mL of phosphate buffer in two separate reaction tubes. 0.5 mL of substrate (0.8 mM) was added to each tube.

Results and discussion

Morphology

To the best of our knowledge, there are no reports of the formation of enzyme–metal–phosphate hybrid nanoflowers or nanopetal structures using ions other than divalent. In this work, precipitates were collected with similar precipitation kinetics, regardless of the metal ions selected for the work. The synthesis resulted in a series of coloured precipitates yellow, light-blue, brown and purple respectively for Fe(II), Cu(II), Ag(I) and Au(III). The coloration clearly indicates the incorporation of the respective metal ions in the precipitates, and potentially indicates the presence of metallic nanoparticles or microparticles of Ag and Au. The morphology, structure and composition of the samples were analysed by SEM, XRD and EDS, using samples collected at different time points and produced using different reaction conditions. The use of metal ions with different valence and/or electronic configuration did not seem to prevent the formation of the characteristic petal-structures, or of nanoflowers, although an effect on morphology was observed under comparable reaction conditions. After 72 hours, all samples presented open, high-surface-area structures (Fig. 1 and ESI†). All enzyme–metal ion combinations resulted in spherical precipitates, albeit under different conditions, of appearance similar to the nanoflowers reported in literature for divalent ions.[25,26,36,37] Variations in the morphology and porosity were observed as function of the reaction conditions (Fig. 1 and ESI†). The growth of the hNFs over time is shown in Fig. 1. After 2 hours precipitates were visible, which at the 24 hour mark seemed to develop into larger petals joined to each other, then turning into more open and fully-formed structures at 72 hours, in line with what previously reported.[25–27,29,38] No major differences were observed in the growth kinetics between the different ions/enzyme mixtures.

Overall, all parameters were observed to affect the morphology and size of the hNFs. The average size of

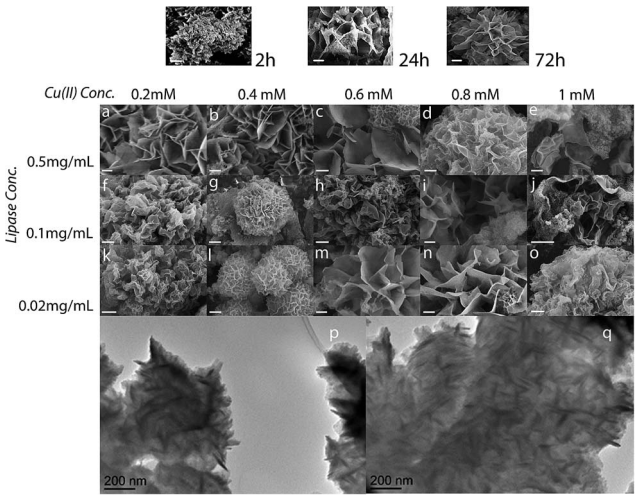

Fig. 1 Top sequence: Growth over time of lipase-hybrid nanoflowers: SEM images of the Cu(II)-lipase hNFs collected at different time points (Cu(II)-0.8 mM, lipase-0.02 mg mL^{-1}, at 21 °C). Below: (a–o) SEM images of Cu(II)-lipase samples incubated at room temperature for 72 h, scale bar: 1 μm; (p and q) bright field TEM images of sample (n) Cu(II)-0.8 mM, lipase-0.02 mg mL^{-1}, at 21 °C.

nanoflowers was measured vary between 3 and 20 μm diameter and the pore size remained in the order of a few microns (calculated as the average distance between petals). The morphology of the precipitate was observed to vary markedly as a function of the reaction conditions. Nanosheets with a few nanoflowers were obtained at high enzyme concentrations (Fig. 1a–e). Spherical nanoflower structures with varied petals size were observed at lower lipase concentration, as a function of the copper sulfate concentration (Fig. 1k–o).

Both SEM and TEM images of Cu(II)-lipase hNFs after 72 hours' reaction at 21 °C show nanoflowers and nanosheets in all samples. TEM analysis revealed the flowers were composed of thin sheets, organised at roughly 120 degrees (Fig. 1p and q).

The nanoflower diameter distribution was measured for one sample prepared at room temperature, 0.8 mM Cu(II) and 0.02 mg mL lipase showing a broad size distribution (ESI†). Cu(II)-lipase samples synthesised at 4 °C, instead, showed unorganised large petals, without clear nanoflower-like arrangement when working at lower copper sulphate concentration and high lipase concentration 0.5 mg mL^{-1}, (ESI†). However, flower-like structures began to appear in samples prepared using low lipase concentrations.

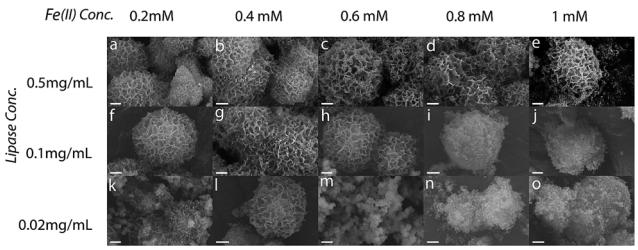

Fig. 2 SEM images of the Fe(II)-lipase hNFs incubated at 4 °C for 72 h, scale bar: 1 μm.

The different working temperatures yielded flower-like precipitates under different reaction conditions, possibly due to the different kinetics of nucleation and growth and the solubility of copper phosphate. These results indicate that temperature conditions during the precipitate formation substantially affected the morphology and structure of the hybrid nanoflowers.

A similar effect of the reaction conditions on nanoflower synthesis was observed for the other metals, in some cases with quite marked differences. For instance, in the case of Fe(II), the effect of temperature with enzyme and metal concentration was more obvious, with 4 °C enabling the synthesis of more homogeneous and aesthetically beautiful flowers (Fig. 2). Open and quite randomly-arranged petal and crystalline structures were instead obtained with Fe(II) at room temperature (ESI†).

The use of non-divalent ions also resulted in porous structures, like for the other ions. Most samples prepared with Ag(I) and Au(III) presented uniform architectures, though often accompanied by crystalline precipitates. Different petal-arrangements were observed by varying the concentrations of lipase and metal ion (Fig. 3 and 4).

Samples prepared using Ag(I) at 21 °C (ESI†), showed properties similar to those seen using copper sulfate and similar reaction conditions, with many nanosheets observed present alongside the nanoflowers at higher enzyme and metal concentrations. At 4 °C, Ag(I) samples appeared more homogeneous across the range of metal ion and enzyme concentrations. Higher metal ion concentrations resulted in the increased presence of crystal structures alongside the nanoflowers, possibly silver chloride.

For Au(III), large thin nanosheets were observed to be present together with a few nanoflowers when the reaction was performed at 21 °C with 0.5 mg mL^{-1} lipase (ESI†), whereas more nanoflower-type precipitates were observed for the lower concentrations, across the spectrum of metal ion concentration. The spherical morphology was also lost for low lipase concentration and high metal ion concentration.

Working at 4 °C yielded quite homogeneous nanoflowers with densely packed nanopetals (Fig. 4). The nanoflowers were observed to be denser at low (0.2 mM) and high (1 mM) gold chloride concentrations.

Energy-dispersive X-ray spectroscopy (EDS) analysis was performed to characterise selected samples (ESI†), and confirmed the presence of: the respective metal ions, phosphorous, as well as carbon and sulphur, which are attributed to

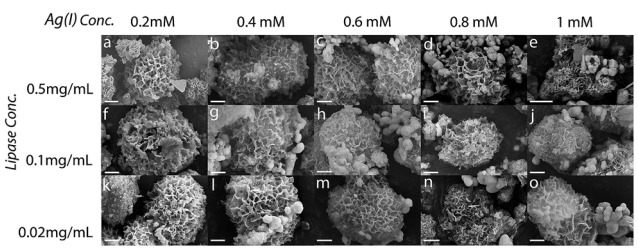

Fig. 3 SEM images of the Ag(I)-lipase hNFs incubated at 4 °C for 72 h, scale bar: 1 μm.

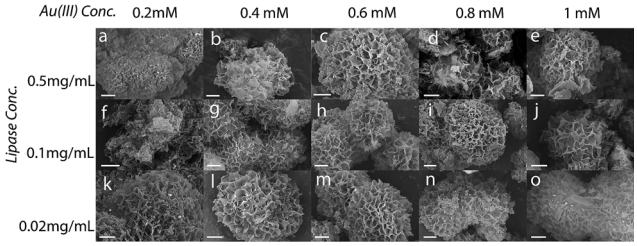

Fig. 4 SEM images of the Au(III)-lipase hNFs incubated at 4 °C for 72 h, scale bar: 1 μm.

the presence of lipase. The sodium peaks in the spectra are likely due to reaction buffer contamination. These results demonstrate that all the different metal ions are present in the hNFs and play a critical role (see morphology results) in the formation of these lipase–metal-ion hNFs.

As illustrated in Fig. 5, FTIR-spectroscopy provides evidence for the composition of the hNFs. Peaks observed at 1650 cm^{-1}, 1350 cm^{-1}, 1460 cm^{-1} and 1020–1220 cm^{-1} are the characteristic of the protein.[32] Typical absorption peaks of native lipase occurred at 1655 and 1541 cm^{-1} for –CONH and 2800–3000 cm^{-1} for $–CH_2$ and $–CH_3$. The same absorption peaks at 1655 and 1541 cm^{-1} and 2800–3000 cm^{-1} were also observed in the spectrum of the hNF. Peaks observed in two particular regions (1700 cm^{-1} to 1600 cm^{-1} and 1550 cm^{-1} to 1500 cm^{-1}) are considered unique to the protein's secondary structure, and are designated as amides I and II, respectively.[39] These results demonstrate that lipase is present within the nanoflowers.[40] Furthermore, strong characteristic peaks of P–O vibrations and stretching were observed at 1052 cm^{-1} and 623 cm^{-1} may be attributed to P–O vibrations, and are considered a proxy for the presence of phosphate groups within the hNF structure.[41] No significant shift in peak positions was observed.

While the presence of the respective phosphate and metal ions were confirmed by EDS and FTIR for all samples, the nature of the phosphate compounds making up the nanoflower remains uncertain for the gold and silver samples. XRD spectra

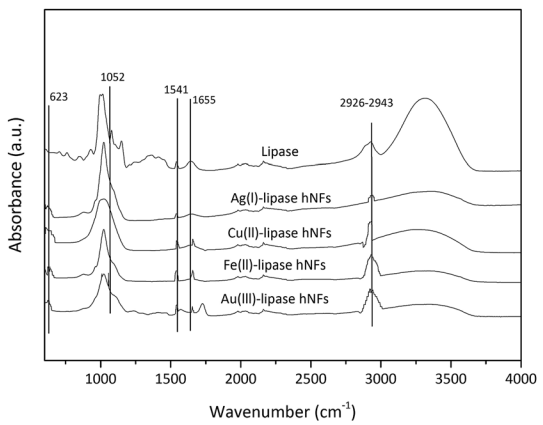

Fig. 5 FTIR spectrum of hNFs synthesised at 4 °C [Fe(II)-lipase hNFs: Fe(II)-(0.6 mM), lipase-(0.1 mg mL^{-1})], synthesised at 21 °C [Cu(II)-lipase hNFs: (Cu(II)-0.8 mM, lipase-0.02 mg mL^{-1}), Ag(I)-lipase hNFs: (Ag(I)-0.4 mM, lipase-0.5 mg mL^{-1}), Au(III)-lipase hNFs: (Au(III)-0.4 mM, lipase-0.02 mg mL^{-1})] and free lipase enzyme.

of the silver-containing and gold-containing samples showed evidence of multiple phases. In particular, the silver-lipase sample showed the presence of silver chloride, $CaHPO_4 \cdot 2H_2O$, and likely Ag_3PO_4, which was difficult to univoquely identify, due to spectral peaks common to those of calcium phosphate (ESI†).[42–44] The gold-lipase sample produced XRD spectra where most peaks seem to be in common with those found in the silver-lipase samples. The position of peaks assigned to $CaHPO_4 \cdot 2H_2O$, though, was observed to be slightly different in the two samples and could indicate doping by gold and silver of the calcium phosphate (ESI†). The presence of gold and silver in the petals of the respective nanoflowers was also confirmed through EDS analysis, indicating that the species are present within the petals, in some form. Nanoparticles of metallic silver and gold were confirmed present by two small peaks (ESI†), finding which provides evidence for the reason behind the coloration of these samples (typical of the respective metallic nanoparticles). Additionally, the presence of AgCl indicates that the product might show photoresponsive properties. In brief, it can be expected that the nanoflowers may contain a variety of metal-based species, including halides, phosphate-complexes, and metallic particles, additionally to surface-bound metal ions. Gold chloride solutions have also been reported to form halophosphate and mixed phosphates (with K(I) or Na(I) or even Ca(II)) when in PBS.[45–47] Since these salts are known to bind to proteins, it can be considered likely that these compounds play a role in the formation of lipase nanoflowers in the presence of Au(III) ions.

It shall suffice to say that the crystalline structure of such compounds to date remains unreported, and that resolving the crystalline structure within the gold-based lipase nanoflowers is a task which warrants separate efforts. Nonetheless, although the nanoflowers containing gold remain of undetermined composition, the effect of the presence of gold ions during nanoflower formation is evident.

Enzymatic activity and stability of hybrid nanoflowers

To determine the enzymatic activity of hNFs, p-nitrophenol palmitate (pnpp) was selected as a model substrate.[33] A marked enhancement in enzymatic activity in respect to free enzyme was observed in most samples (ESI†), with the highest activities measuring: 1463 U mg^{-1} (iron-lipase hNFs), 1522 U mg^{-1} (copper-lipase hNFs), 1567 U mg^{-1} (silver-lipase hNFs) and 1483 U mg^{-1} (gold-lipase hNFs). These values indicate that the specific activity of lipase hNFs is ~5-fold that of free lipase. This finding is consistent with the findings of previous studies by Cui, *et al.* who observed that surfactant-activated lipase–inorganic hNF exhibited 4.6-fold the activity of free lipase in solution.[40] Ke, *et al.* also found that the activity of lipase-inorganic hNF was 3-fold that of free lipase.[32] Ocsoy, *et al.* reported that Fe(II)-HRP hybrid nanoflowers with 7 times the catalytic activity of free enzyme.[31] Importantly, it was observed that the difference in activity as a function of metal type and ion concentration was small, and is here considered negligible, indicating that the morphology of the hNFs was not sensibly affecting the specific activity of the enzyme.

Although the molecular distribution and the interactions between lipase molecules and the phosphate and metal ions warrant further research, the enhanced activity reported in all samples containing the three components is evidence of their synergistic effect in favourably presenting the enzyme in the reaction.

The stability of the hNFs was also assessed by performing enzyme assays after storing the hNFs at different temperatures for 21 days. It was observed that the hNFs stored at 4 °C and 21 °C for 21 days respectively retained 94% and 70% of their original activities. By comparison, the same concentration of free lipase stored at 4 °C and 21 °C respectively retained 29%

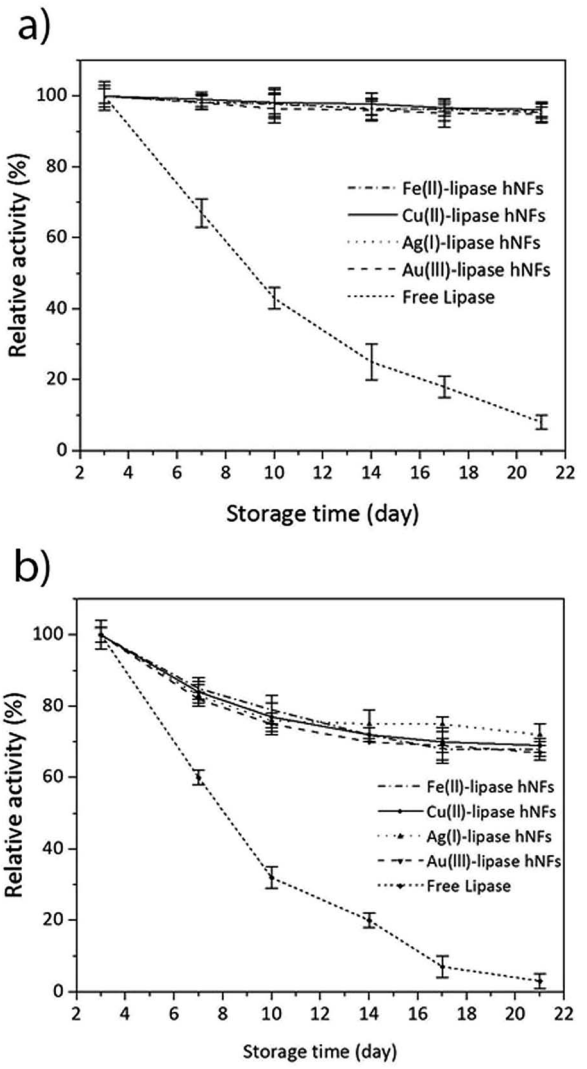

Fig. 6 Stability of hNFs and free lipase enzyme towards pnpp. (a) Storage at 4 °C, for samples synthesised at 4 °C [Fe(II)-lipase hNFs: Fe(II)-(0.6 mM), lipase-(0.1 mg mL^{-1})], and synthesised at 21 °C [Cu(II)-lipase hNFs: (Cu(II)-0.8 mM, lipase-0.02 mg mL^{-1}), Ag(I)-lipase hNFs: (Ag(I)-0.4 mM, lipase-0.5 mg mL^{-1}), Au(III)-lipase hNFs: (Au(III)-0.4 mM, lipase-0.02 mg mL^{-1})] and free lipase enzyme. (b) Storage at 21 °C of samples synthesised at 4 °C: [Fe(II)-lipase hNFs: Fe(II)-(0.6 mM), lipase-(0.1 mg mL^{-1})], and synthesised at 21 °C [Cu(II)-lipase hNFs: (Cu(II)-0.8 mM, lipase-0.02 mg mL^{-1}), Ag(I)-lipase hNFs: (Ag(I)-0.4 mM, lipase-0.5 mg mL^{-1})] and free lipase enzyme.

and 7% of the original activity (Fig. 6A and B). This result indicates that the enzyme within hNFs is stabilised. This is in line with what was previously observed in the literatures. Yan, *et al.* reported that hNFs maintained more than 75% activity after 16 days.[32] The reusability of the enzyme in the hNFs also seemed improved (Fig. 7), with each type of hNFs maintaining around 75% of the original activity after six uses in functional assays. This finding is consistent with the study by Yan *et al.*,[32] who found that lipase-hNFs maintained around 80% activity after five uses. The research finding by Cui, *et al.*[40] also indicates similar reusability results for lipase-hNFs.

The hNFs were also tested for enzyme activity against different short chain fatty acids to verify substrate specificity. Under optimised temperature (40–50 °C) and substrate (natural oils) conditions, the yield of transesterification catalysed by lipases exceeds 83–87%.[48–52] As shown in Fig. 7, the results suggest that ferrous-lipase, silver-lipase and gold-lipase hNFs showed maximum activity by using decanoic acid (C10), whereas copper-lipase hNFs and free lipase showed the highest activity by using palmitic acid (C16). Differences in substrate specificity may indicate different orientation of the enzyme in its immobilised form, and result in different suitability of the different nanoflowers for industrial applications.

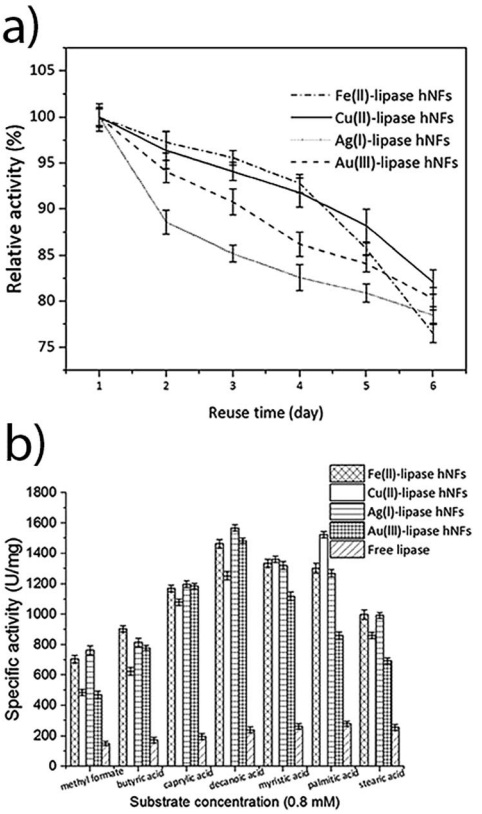

Fig. 7 (a) Reusability study of the hNFs. [Synthesised at 4 °C [Fe(II)-lipase hNFs: Fe(II)-(0.6 mM), lipase-(0.1 mg mL^{-1})], synthesised at 21 °C [Cu(II)-lipase hNFs: (Cu(II)-0.8 mM, lipase-0.02 mg mL^{-1}), Ag(I)-lipase hNFs: (Ag(I)-0.4 mM, lipase-0.5 mg mL^{-1}), Au(III)-lipase hNFs: (Au(III)-0.4 mM, lipase-0.02 mg mL^{-1})] and free lipase enzyme. Each value represents the mean of three independent determinations. Error bars indicate the standard deviation; (b) effect of substrate hydrolysis on hNFs synthesised at 4 °C [Fe(II)-lipase hNFs: Fe(II)-(0.6 mM), lipase-(0.1 mg mL^{-1})], synthesised at 21 °C [Cu(II)-lipase hNFs: (Cu(II)-0.8 mM, lipase-0.02 mg mL^{-1}), Ag(I)-lipase hNFs: (Ag(I)-0.4 mM, lipase-0.5 mg mL^{-1}), Au(III)-lipase hNFs: (Au(III)-0.4 mM, lipase-0.02 mg mL^{-1})] and free lipase enzyme.

Conclusions

This study has demonstrated that lipase-containing nanoflowers can be prepared starting from a variety of metal ions, not just di-valent, and in a wide range of conditions. Different shapes of nanostructures can be generated: loosely-arranged flower-like nanopetals, densely packed nanoflowers, nanosheets and thick nanopetals. All metal ions were found to produce nanoflowers, albeit under different conditions, and all samples presented specific activity of the same order of magnitude, regardless of their morphology. While previous literature has focused on the optimisation of the structural features of nanoflowers, this study indicates that the macromorphology of the porous precipitate is not a major determining factor in the enzymatic activity of the samples.

High specific activity, high enzyme reusability and improved stability were measured for all samples prepared in this work, without metal-ion specificity. This indicates that the type of metal ion and the macroscopic arrangement of the petals play a secondary role in determining lipase activity to that of the co-presence of metal and phosphate ions and enzyme. Although further research is required to elucidate the crystalline forms of some nanoflower compositions, these results also clearly indicate that the phosphate–metal-ion–enzyme system is very robust, and in particular that more "courageous choices" in the selection of metal ions other than Ca(II), Cu(II) and Fe(II) can be attempted.

Literature on the formation of nanoflowers has so far only focused on di-valent ions, but the results presented here indicate that possibly it is the insolubility of metal phosphates and their protein-complexes that allows precipitation and growth of these structures. The option to use different valence and different metals is expected to have important consequences in opening up new areas of metal–phosphate–protein research. Although indicating that multiple ion combinations can be used in this approach, this study points towards a need to further study the effect of the co-presence of metal ions such as Ca(II) and the transition metal ions, and to investigate the effect of chloride and other counterions on the formation of the nanoflowers and their resulting activity.

Since certain enzymes and proteins are, for instance, intolerant of the co-presence of certain metal ions, such as Cu(II) or Ca(II), and show reduced activity, the ability to produce nanostructures with different metal ions, demonstrated here, will likely open the way to a wider range of enzyme–metal–phosphate systems, not possible before.

Acknowledgements

This work was supported in part by the Australian Research Council World Class Future Fibre Industry Transformation Research Hub (IH140100018) and in part by the Advanced

Manufacturing Cooperative Research Centre (Project #1.2.4.2). The present work was carried out with the support of the Deakin Advanced Characterisation Facility. The authors are grateful to Dr Adam Taylor and Dr Andrew Sullivan for their support in acquiring the EDS spectra for this work.

References

1 J. Kim, J. W. Grate and P. Wang, *Trends Biotechnol.*, 2008, **26**, 639–646.
2 J. Ge, D. Lu, Z. Liu and Z. Liu, *Biochem. Eng. J.*, 2009, **44**, 53–59.
3 B. Krajewska, *Enzyme Microb. Technol.*, 2004, **35**, 126–139.
4 R. Messing, *Immobilized enzymes for industrial reactors*, Elsevier, 2012.
5 P. Wang, *Curr. Opin. Biotechnol.*, 2006, **17**, 574–579.
6 K. Matsumoto, B. G. Davis and J. B. Jones, *Chem.–Eur. J.*, 2002, **8**, 4129–4137.
7 M. Puri, C. J. Barrow and M. L. Verma, *Trends Biotechnol.*, 2013, **31**, 215–216.
8 B. G. Davis, X. Shang, G. DeSantis, R. R. Bott and J. B. Jones, *Bioorg. Med. Chem.*, 1999, **7**, 2293–2301.
9 H. Grøn, L. M. Bech, S. Branner and K. Breddam, *Eur. J. Biochem.*, 1990, **194**, 897–901.
10 R. Abdulla and P. Ravindra, *Biomass Bioenergy*, 2013, **56**, 8–13.
11 W. Hartmeier, *Trends Biotechnol.*, 1985, **3**, 149–153.
12 P. Johnson, H. Park and A. Driscoll, in *Enzyme Stabilization and Immobilization*, ed. S. D. Minteer, Humana Press, 2011, ch. 15, vol. 679, pp. 183–191.
13 A. Talebian-Kiakalaieh, N. A. S. Amin and H. Mazaheri, *Appl. Energy*, 2013, **104**, 683–710.
14 W. Tischer and V. Kasche, *Trends Biotechnol.*, 1999, **17**, 326–335.
15 M. Verma, W. Azmi and S. Kanwar, *Acta Microbiol. Immunol. Hung.*, 2008, **55**, 265–294.
16 L. Cao, *Curr. Opin. Chem. Biol.*, 2005, **9**, 217–226.
17 Y. Z. Chen, C. B. Ching and R. Xu, *Process Biochem.*, 2009, **44**, 1245–1251.
18 C. Mateo, J. M. Palomo, G. Fernandez-Lorente, J. M. Guisan and R. Fernandez-Lafuente, *Enzyme Microb. Technol.*, 2007, **40**, 1451–1463.
19 S. A. Ansari and Q. Husain, *Biotechnol. Adv.*, 2012, **30**, 512–523.
20 A. S. Aricò, P. Bruce, B. Scrosati, J.-M. Tarascon and W. Van Schalkwijk, *Nat. Mater.*, 2005, **4**, 366–377.
21 S. Becker, *J. Nanopart. Res.*, 2013, **15**, 1–13.
22 J. Kim and J. W. Grate, *Nano Lett.*, 2003, **3**, 1219–1222.
23 J. Kim, J. W. Grate and P. Wang, *Chem. Eng. Sci.*, 2006, **61**, 1017–1026.
24 Z.-G. Wang, L.-S. Wan, Z.-M. Liu, X.-J. Huang and Z.-K. Xu, *J. Mol. Catal. B: Enzym.*, 2009, **56**, 189–195.
25 J. Ge, J. Lei and R. N. Zare, *Nat. Nanotechnol.*, 2012, **7**, 428–432.
26 Z. Lin, Y. Xiao, Y. Yin, W. Hu, W. Liu and H. Yang, *ACS Appl. Mater. Interfaces*, 2014, **6**, 10775–10782.
27 B. Somturk, M. Hancer, I. Ocsoy and N. Ozdemir, *Dalton Trans.*, 2015, **44**, 13845–13852.
28 B. Somturk, I. Yilmaz, C. Altinkaynak, A. Karatepe, N. Ozdemir and I. Ocsoy, *Enzyme Microb. Technol.*, 2016, **86**, 134–142.
29 L. Zhu, L. Gong, Y. Zhang, R. Wang, J. Ge, Z. Liu and R. N. Zare, *Chem.–Asian J.*, 2013, **8**, 2358–2360.
30 Z. Wu, X. Li, F. Li, H. Yue, C. He, F. Xie and Z. Wang, *RSC Adv.*, 2014, **4**, 33998–34002.
31 I. Ocsoy, E. Dogru and S. Usta, *Enzyme Microb. Technol.*, 2015, **75–76**, 25–29.
32 C. Ke, Y. Fan, Y. Chen, L. Xu and Y. Yan, *RSC Adv.*, 2016, **6**, 19413–19416.
33 S.-S. Yi, J.-M. Noh and Y.-S. Lee, *J. Mol. Catal. B: Enzym.*, 2009, **57**, 123–129.
34 M. B. Marion, *Anal. Biochem.*, 1976, **72**, 248–254.
35 S. S. Dhiman, D. Kalyani, S. S. Jagtap, J.-R. Haw, Y. C. Kang and J.-K. Lee, *Appl. Microbiol. Biotechnol.*, 2013, **97**, 1081–1091.
36 J. Sun, J. Ge, W. Liu, M. Lan, H. Zhang, P. Wang, Y. Wang and Z. Niu, *Nanoscale*, 2014, **6**, 255–262.
37 X. Wang, J. Shi, Z. Li, S. Zhang, H. Wu, Z. Jiang, C. Yang and C. Tian, *ACS Appl. Mater. Interfaces*, 2014, **6**, 14522–14532.
38 R. Wang, Y. Zhang, D. Lu, J. Ge, Z. Liu and R. N. Zare, *Wiley Interdiscip. Rev.: Nanomed. Nanobiotechnol.*, 2013, **5**, 320–328.
39 S. Li, J. D. Combs, O. E. Alharbi, J. Kong, C. Wang and R. M. Leblanc, *Chem. Commun.*, 2015, **51**, 12537–12539.
40 J. Cui, Y. Zhao, R. Liu, C. Zhong and S. Jia, *Sci. Rep.*, 2016, **6**, 27928.
41 Y. Yu, X. Fei, J. Tian, L. Xu, X. Wang and Y. Wang, *Colloids Surf., B*, 2015, **130**, 299–304.
42 Z. Yi, J. Ye, N. Kikugawa, T. Kako, S. Ouyang, H. Stuart-Williams, H. Yang, J. Cao, W. Luo, Z. Li, Y. Liu and R. L. Withers, *Nat. Mater.*, 2010, **9**, 559–564.
43 K. Baďurová, O. Monfort, L. Satrapinskyy, E. Dworniczek, G. Gościniak and G. Plesch, *Ceram. Int.*, 2017, **43**, 3706–3712.
44 L. C. Natale, Y. Alania, M. C. Rodrigues, A. Simões, D. N. de Souza, E. de Lima, V. E. Arana-Chavez, T. L. R. Hewer, R. Hiers, F. L. Esteban-Florez, G. E. S. Brito, S. Khajotia and R. R. Braga, *Mater. Sci. Eng., Proc. Conf.*, 2017, **76**, 464–471.
45 L. Schmued and W. Slikker Jr, *Brain Res.*, 1999, **837**, 289–297.
46 L. Schmued, J. Bowyer, M. Cozart, D. Heard, Z. Binienda and M. Paule, *Brain Res.*, 2008, **1229**, 210–217.
47 L. C. Schmued, US Pat.,US 6372451 B1, 2002.
48 W. Du, Y.-Y. Xu, D.-H. Liu and Z.-B. Li, *J. Mol. Catal. B: Enzym.*, 2005, **37**, 68–71.
49 H. Jia, in *Nanoscale Biocatalysis*, Springer, 2011, pp. 205–212.
50 L. A. Nelson, T. A. Foglia and W. N. Marmer, *J. Am. Oil Chem. Soc.*, 1996, **73**, 1191–1195.
51 M. M. Soumanou and U. T. Bornscheuer, *Enzyme Microb. Technol.*, 2003, **33**, 97–103.
52 Y. Watanabe, Y. Shimada, A. Sugihara and Y. Tominaga, *J. Mol. Catal. B: Enzym.*, 2002, **17**, 151–155.